# Polyol-Mediated Solvothermal Synthesis and Electrochemical Performance of Nanostructured V$_2$O$_5$ Hollow Microspheres

Evan Uchaker, Nan Zhou, Yanwei Li, and Guozhong Cao*

Department of Materials Science & Engineering, University of Washington, Seattle, Washington, 98195, United States

🅢 Supporting Information

ABSTRACT: Hollow vanadyl glycolate nanostructured microspheres were synthesized via a highly scalable and template-free polyol-induced solvothermal process. Subsequent calcination transformed the precursor material into vanadium pentoxide, a well-studied transition metal oxide. The vanadyl glycolate nanoparticles were synthesized through a self-seeding process and then aggregated around N$_2$ microbubbles formed during the reaction that acted as "quasi-micelles" due to the large polarization discrepancy between nitrogen and water. The proposed formation mechanism provides a firm understanding of the processes leading to the observed hollow microsphere morphology. The thermally treated material was tested as a cathode for lithium-ion battery and showed excellent cycle stability and high rate performance. The exceptional electrochemical performance was attributed to the relatively thin-walled structure that ensured fast phase penetration between the electrolyte and active material and shortened lithium-ion migration distance. The prolonged cycling stability is ascribed to the inherent morphological void that can readily accommodate volume expansion and contraction upon cycling.
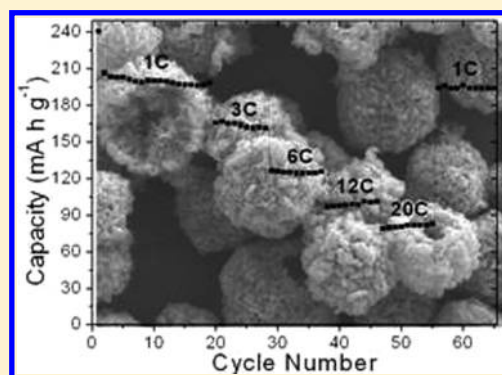
■ INTRODUCTION

Self-assembled nanostructures with particular morphology and specific properties have been the subject of intense research over the past several decades due to their novel properties and tunable functions that can be utilized in a wide range of applications.[1−3] The use of organic surfactants and polymers in nanoparticle synthesis has been a popular method of achieving morphological control, where the polymer or foreign ions typically work to regulate and stabilize the surface of the nanoparticles.[4] One of the most common and facile approaches that utilize this technique is the polyol method. Initial studies concerning the polyol method focused on the preparation of elemental metals and alloys by exploiting the reducing properties of a high-boiling alcohol (i.e., glycerol or glycol) towards a suitable metal precursor. The alcohol often acts as a stabilizing agent that effectively limits particle growth and hinders aggregation.

The polyol process is heralded for its self-seeding mechanism and lack of required "hard" or "soft" templating materials, making it an ideal process for potential industrial scale-up due to the low cost and ease of processing.[5,6] Over the past several years, the number of oxide material systems synthesized via the polyol method has steadily increased; several reports have summarized the polyol method of oxide materials as a sol−gel process carried out at elevated temperature that is suitable for the preparation of a host of binary and ternary oxides.[7] The polyol process has since been utilized for the synthesis of a wide range of metal oxide materials, including V$_x$O$_y$,[8] TiO$_2$,[9] PbO, and SnO$_2$.[10] Several investigations have considered the role of the inorganic species in controlling the shape of metal and metal oxide nanoparticles, as they may provide as powerful a means as organic surfactants and polymers for controlling the shape of the synthesized nanoparticles.[11−16]

Ethylene glycol (EG) is among one of the most widely used solvents for the polyol synthesis of metal and metal oxide nanoparticles due to its strong reducing capability, relatively high boiling point (∼197 °C), and high dielectric constant which increases the solubility of inorganic salts.[17,18] EG is commonly used as a cross-linking reagent because of its propensity to coordinate to the central metal ion and form a metal glycolate, leading to subsequent oligomerization.[19] Herricks et al. revealed that for the formation of platinum (Pt) nanowires the critical factor dictating the morphological control was the nitrate anion, whose function was to substantially slow the reduction of Pt(II) and Pt(IV) species in EG.[16] Jiang et al. demonstrated that EG is an effective reagent in the formation of various metal oxide nanowires that formed a chain-like precursor after refluxing a suitable metal salt in EG.[10] It was also determined that the as-synthesized glycolate precursors could later be converted to their more common metal oxide derivatives when calcined in air, all while maintaining the original precursor morphology. Such was the formation mechanism for the fabrication of titanium oxide, tin dioxide, zirconium oxide, and niobium oxide mesostructures.[10]

In this study, a simple and convenient method has been developed for the large-scale synthesis of nanostructured V_2O_5 hollow microspheres with diameters of approximately 3.0 μm. A great deal of recent research efforts have been focused on the study of hollow nanostructured materials, such as nanotubes and hollow spheres, that demonstrate unique characteristics due to their distinct morphology.[20] Hollow nanostructured materials have been known to exhibit large surface area, low density, and enhanced surface permeability because of their inner voids; such materials have been used in a wide range of applications, including lithium-ion (Li-ion) batteries, catalysts, optoelectronic sensors, and drug-delivery systems.[21,22] Nanostructured vanadyl glycolate microspheres were first formed via the polyol process and then converted to orthorhombic crystalline V_2O_5 by calcining in air at elevated temperature. The glycolate precursor was transformed into the corresponding metal oxide without experiencing any change in morphology. Electron microscopy and diffraction studies were used to characterize the morphology, crystallinity, and structure of the hollow nanostructured microspheres. The highly monodisperse product was ultimately tested as a Li-ion battery cathode material and showed excellent stability and high-rate reversible capacity upon cycling.

■ EXPERIMENTAL PROCEDURE

Nanostructured V_2O_5 hollow microspheres were synthesized via a solvothermal route followed by thermal treatment. In brief, 0.1754 g of ammonium metavanadate (NH_4VO_3, Sigma Aldrich) was stirred in 20 mL of ethylene glycol ($H_2C_6O_2$, VWR) for 8 h. The solution was loaded into a 50 mL polytetrafluoroethylene (PTFE) lined stainless steel autoclave and then solvothermally treated for 24 h at 180 °C, after which it was cooled naturally. Following precipitate isolation and drying, the samples were annealed at 500 °C for 2 h in air.

The phase and crystallite size of the V_2O_5 microspheres were studied using X-ray diffraction (XRD, D8 Bruker X-ray diffractometer); the sample was scanned with Cu−K_α radiation within the range of 10°−70° (2θ), with a step size of 0.02° and an exposure time of 10 s. The accelerating voltage and current were 40 kV and 40 mA, respectively. Infrared absorption spectra were recorded using a Perkin-Elmer 1640 Fourier Transform Infrared (FTIR, Perkin-Elmer) spectrophotometer with KBr pellets. The surface morphology of the microspheres was examined using scanning electron microscopy (SEM, JEOL JSM-7000F). Transmission electron microscopy (TEM) was carried out using an FEI Tecnai G2 F20 operating at 200 kV after the samples had been embedded in Araldite 502 (SPI-Chem) epoxy resin and then cut to 100 nm thick segments using a Leica EM UC6 ultramicrotome. The nitrogen sorption was performed using a Quantachrome NOVA 4200e. The specific surface area and micropore and mesopore volumes were determined using multipoint Brunauer−Emmett−Teller (BET), t-method, and Barrett−Joyner−Halenda (BJH) desorption analyses, respectively.

The electrode slurry was prepared by mixing the annealed V_2O_5 microsphere powder, Super P conductive carbon (TIMCAL Graphite & Carbon), and polyvinylidene fluoride (PVDF) binder dispersed in a N-methyl-2-pyrrolidone (NMP, Alfa Aesar) solution at a respective weight ratio of 80:12:08. The slurry was spread onto aluminum foil and dried in a vacuum oven at 80 °C overnight prior to coin-cell assembly. The 2032 type half-cells were assembled in a glovebox (MTI Corp.) filled with ultrahigh purity argon. Lithium metal foil, 1 M $LiPF_6$ in ethylene carbonate (EC)/dimethyl carbonate (DMC) (1:1 v/v), and Celgard 2400 membrane were used as the counter/reference electrode, electrolyte, and separator, respectively. Cyclic voltammetry (CV) was completed using an electrochemical analyzer (CH Instruments, model 605B) in the voltage range of 2.0−4.0 V (vs Li/Li⁺) at a scan rate of 0.2 mV s⁻¹. The current density and cycle stability performance of the V_2O_5 microspheres were evaluated using an Arbin Battery Tester (BT-2000, Arbin Instruments) operating at room temperature. The half-cells were tested within the voltage range of 2.0−3.8 V vs Li/Li⁺ at various charging rates based on the weight of the active material alone and assuming a 1C current density of 294 mA g⁻¹.

■ RESULTS AND DISCUSSION

The XRD and FTIR spectra of the pre- and post-calcined samples are shown in Figure 1. Prior to calcination, the phase
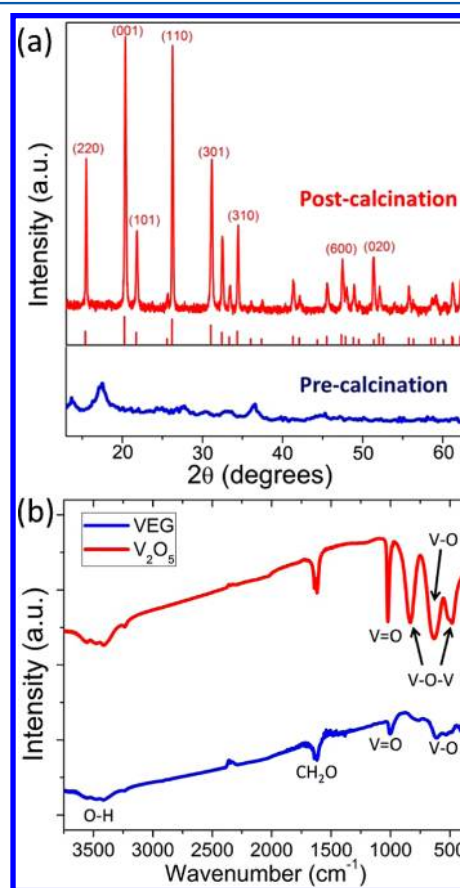

Figure 1. Respective (a) XRD and (b) FTIR spectra of the pre- and post-calcined vanadyl glycolate (VEG) and V_2O_5 microspheres.

was indexed as vanadyl glycolate, $VO(CH_2O)_2$, with some potential hydrogen or carbon additions.[8] Following the calcination step, the microsphere morphology of the sample was preserved and could be indexed to the orthorhombic form of vanadium oxide, V_2O_5 (space group: Pmmn (59), a = 11.516, b = 3.566, c = 3.777 Å; JCPDS card no. 41-1426). The transition from the vanadyl glycolate precursor to crystalline V_2O_5 was also noted by the sample changing color from black (pre-calcined) to orange (post-calcined).

The transformation from the vanadyl glycolate precursor to V_2O_5 was also confirmed by means of FTIR, as shown in Figure

1b. In the vanadyl glycolate curve, the peak centered at 3412 cm^{-1} corresponds to the O−H stretching band, and the peak at 1628 cm^{-1} corresponds to the $[CH_2O]$ group of the vanadyl glycolate compound. Similarly, the peak centered at 1005 cm^{-1} can be assigned to the V=O stretching bond, and the peaks centered at 761 and 611 cm^{-1} potentially originate from the V−O bond. For V_2O_5, the V=O stretching bond appears at 1022 cm^{-1}, whereas the peaks at 509 and 834 cm^{-1} are attributed to the symmetric and asymmetric stretching of the V−O−V bond, respectively. The peak at 631 cm^{-1} corresponds to the stretching of the V−O bond, while the 836 cm^{-1} peak can be attributed to the coupled vibration between the V=O and V−O−V bonds.[8,23] Comparison with the V_2O_5 spectra demonstrates that many of the absorption peaks corresponding to the vanadyl glycolate complex disappear following calcination. The V=O vibrational bonds tend to shift to higher wavenumbers with increasing valence of the vanadium species, from 1005 cm^{-1} for vanadyl glycolate to 1022 cm^{-1} for V_2O_5. This vibration shift is most likely caused by the increase in the number of electron-withdrawing groups (O) surrounding the V=O group since the transformation from vanadyl glycolate to V_2O_5 is an oxidation process ($V^{4+} => V^{5+}$), where the increase in the vanadium species valence state shifts the V=O bond vibrations to higher wavenumbers.

SEM results demonstrated that a monodisperse, non-agglomerated, high yield product can be achieved employing the described solvothermal, template-free synthesis technique. The collected SEM micrographs also show that the hollow microspheres, with an average outer diameter of approximately 3.0 μm and an inner diameter of approximately 750 nm, were composed of aggregated nanoparticles both before and after calcination. The size of the individual nanoparticles that formed the hierarchical aggregate nanostructure ranged from 60 to 110 nm and was confirmed with a calculated average size of 77 nm as determined by applying the Scherrer equation to the full width at half-maximum of the (001) peak from the XRD spectrum. Cross-sectional TEM characterization further confirms the size of the individual nanoparticles and that the aggregated microspheres are hollow (Figures 2d and S1, Supporting Information).
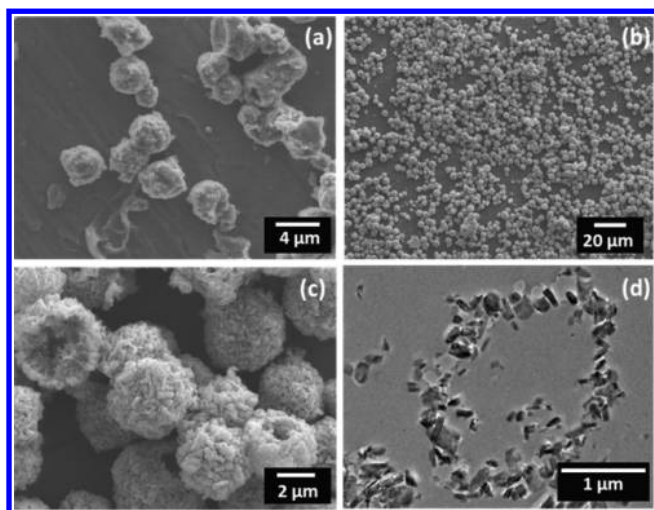

Figure 2. SEM images of the (a) pre-calcined vanadyl glycolate microspheres; (b, c) SEM and (d) cross-sectional TEM images of the post-calcined hollow V_2O_5 nanostructured microspheres.

The BJH pore size distribution (Figure S2, Supporting Information) obtained from the adsorption−desorption isotherm suggests that the V_2O_5 sample contains broadly distributed pores with sizes below 10 nm, the majority of which are in the 5−8 nm size range. The BET specific surface area was approximated to be 21.9 $m^2 g^{-1}$, which is a reasonable value for materials containing pores on the aforementioned scale. The relatively large surface area of the prepared porous V_2O_5 nanostructures ensures short Li-ion diffusion distances and therefore holds the potential for enhanced electrochemical performance.[24]

The polyol process, or use of polyol or diol as the reducing reagent, has been widely applied to reduce metal salts to metal nanoparticles and is typically used in combination with a surfactant to control particle morphology.[12] However, it has also been established that inorganic species may provide a means as powerful as organic surfactants and polymers for controlling the shape of metallic and metal oxide nanoparticles.[11−15] The reaction between NH_4VO_3 and EG has been previously documented by Ragupathy et al.,[8] who used the precursor materials to synthesize vanadyl glycolate via the polyol reaction method that was transformed to V_2O_5 nanostrips with subsequent calcination according to:

$$NH_4VO_3 + C_2H_6O_2 = >N_2 + VO(CH_2O)_2 + H_2O \tag{1}$$
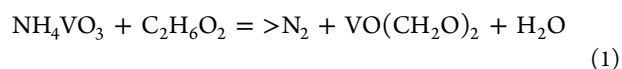
The vanadyl glycolate structure is comprised of one-dimensional chains that contain edge sharing VO_5 square pyramids. The oxygen atoms within the chain derive from a vanadyl group, a chelating ($-OCH_2CH_2O-$) ligand, and one end of two other ($-OCH_2CH_2O-$) ligands present, as shown in Figure 3a.
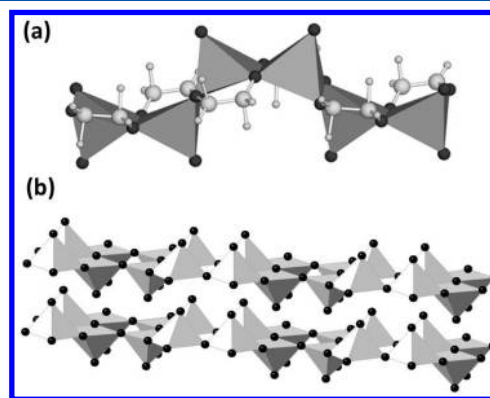

Figure 3. Structures of (a) vanadyl glycolate and (b) V_2O_5. Figure 3a is reproduced from ref 25 with permission from The Royal Society of Chemistry.

In this study, ethylene glycol served as both the solvent and the reducing agent for the reaction.[4] Ethylene glycol has been established as a cross-linking reagent and has been used for the controlled synthesis of metal nanoparticles.[11,16,26,27] Xia and co-workers proposed that the synthesis of metal nanoparticles in the presence of EG occurs in two steps: (1) coordination of EG to the central metal ion to form a metal glycolate and (2) subsequent oligomerization.[16] In the presence of the reducing agent, a bimodal distribution of vanadyl glycolate nanoparticles will form through a self-seeding process, followed by subsequent homogeneous and heterogeneous nucleation. Formation of the nanoparticles proceeds through two separate
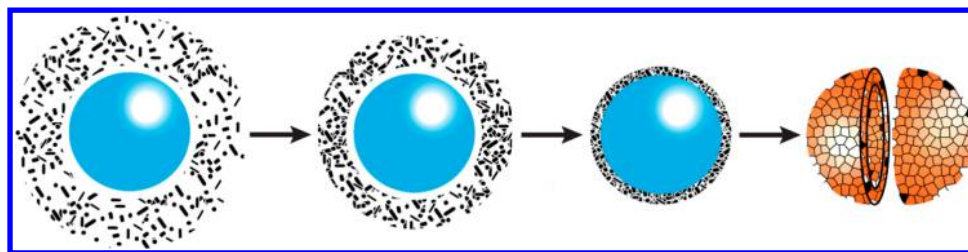
Figure 4. Schematic depicting the formation of vanadyl glycolate nanoparticle aggregated hollow microspheres (cross-sectional view) and the resulting V_2O_5 nanoparticle aggregated hollow microspheres following calcination.

steps: a very short nucleation step followed by a particle growth step controlled either by the kinetics of the chemical reaction or the interfacial diffusion of the reacting species. Over the course of the solvothermal growth process, Ostwald ripening will manage the size of the nanoparticles with larger particles growing at the expense of their smaller counterparts.[26] In essence, the nanoparticles initially nucleate and then grow with the oligomerization of vanadyl glycolate via the LaMer scheme.[28]

It is proposed that the hollow microsphere morphology of the aggregated vanadyl glycolate nanoparticles can be attributed to the formation of N_2 microbubbles, formed in accordance with eq 1. The vanadyl glycolate nanoparticles aggregate around the N_2 microbubbles produced during the reaction in an attempt to minimize their interfacial energy (Figure 4).[29] The aggregation reaction can be likened to the case where a templating surfactant, such as polyvinylpyrrolidone (PVP), is used. The templating nature of PVP can be ascribed to the hydrophobic vinyl group and hydrophilic carbonyl group that lead to the formation of polarized micelles. Hollow microspheres of vanadium oxide were previously formed through a polyol reaction involving vanadium(III) acetylacetonate (acac), where PVP assisted in the formation of spherical micelles in EG.[30] The carbonyl groups of the PVP chains face outward, and the bidentate $[C_5H_8O_2]$ ligand of $[V(acac)_3]$ is gradually replaced by EG to form vanadyl glycolate, which can be easily adsorbed onto the micelle surface through the abundant hydroxy groups.

While no templating agents were used in this study, the N_2 microbubbles act as "quasi-micelles" because of the difference in the polarizability of the phases during solvothermal synthesis. As opposed to directly measuring the polarization value, it is possible to compare the dielectric constant of the two phases since the dielectric constant scales with polarization ($D = \varepsilon_o E + P$); the dielectric constant for H_2O and N_2 at room temperature is 80.4 (34.5 at 200 °C) and 1.0 (1.4 at 170 °C), respectively. Aggregation of the vanadyl glycolate nanoparticles around the N_2 microbubbles is driven by this large difference in polarization between H_2O and N_2 and the incentive for the nanoparticles to decrease their interfacial energy at the solid–liquid interface. Once enough particles coat the microbubble, the structure can become self-supporting and incredibly stable as proven by the microscopy and electrochemical results. This aggregation process has been previously reported for the formation of various monodispersed oxide particles,[31] where the driving force for the colloid particle reorganization corresponds to a reduction in the surface free energy. Such a mechanism may be equipped to explain the formation and morphology of the vanadyl glycolate precursors, and eventual V_2O_5 metal oxide, synthesized in this study.

It should be noted that the morphology of the individual nanoparticles was altered from nanorods to nanoparticles upon transitioning from vanadyl glycolate to V_2O_5. This small change in the morphology can be attributed to the nanorods disassembling during the annealing process because of lattice mismatch and accompanying strain experienced during the transformation process. Ostwald ripening and, a slight degree of, sintering then took place, producing the V_2O_5 nanoparticles; however, the morphology and size of the aggregated microspheres remained the same. Figure S3 (Supporting Information) displays the growth process as examined by harvesting the synthesized products at different reaction time intervals. Complete vanadyl glycolate microspheres were nearly formed even after 1 h of solvothermal growth; subsequently collected specimens show that the individual particles coarsened with time, but the overall sphere morphology and size became more monodisperse.

The V_2O_5 structure can be viewed as corner- and edge-sharing VO_6 octahedra (Figure 3b), where the octahedra are irregular with five V–O distances ranging from 0.159 and 0.202 nm with a sixth distance as large as 0.279 nm,[32] leading to a large V–O separation along the crystallographic c-direction. Because of the varying V–O distances, it is possible to describe the structure as layered square VO pyramids, with five oxygen atoms surrounding the vanadium atom and the separation distance between each layer depending on the water content of the compound. Ultimately, these factors all make the layered structure of V_2O_5 ideal for functioning as an intercalation host,[32,33] which is why the compound has been extensively studied since being reported by Whittingham.[33] A wide assortment of V_2O_5 nanostructures have already been synthesized by a variety of methods, including reverse-micelle transition, sol–gel processing, hydrothermal treatment, and electrochemical deposition.[34]

The intercalation of V_2O_5 occurs with compensating electrons leading to the formation of vanadium bronzes and can be expressed as $V_2O_5 + x\text{Li}^+ + xe^- \leftrightarrow \text{Li}_xV_2O_5$ when lithium is the intercalating species. V_2O_5 has a reversible capacity of 294 mA h g^{-1} that corresponds to the intercalation of two Li$^+$ per formula unit before the transition to the Li$_3$V$_2$O$_5$ irreversible phase occurs; however, V_2O_5 is notoriously known for its poor cycle stability. One method of overcoming the poor cyclic stability is by employing hollow nanostructured materials, such as hollow microspheres, as the electro-active material of the electrode. Hollow nanostructured materials have been known to exhibit large surface area, low density, and enhanced surface permeability because of their inner cavities. The morphological void of hollow nanostructured materials is the feature responsible for enhancing the electrochemical performance in two ways. First, the void within hollow nanostructured materials may alleviate any localized volume change experi-
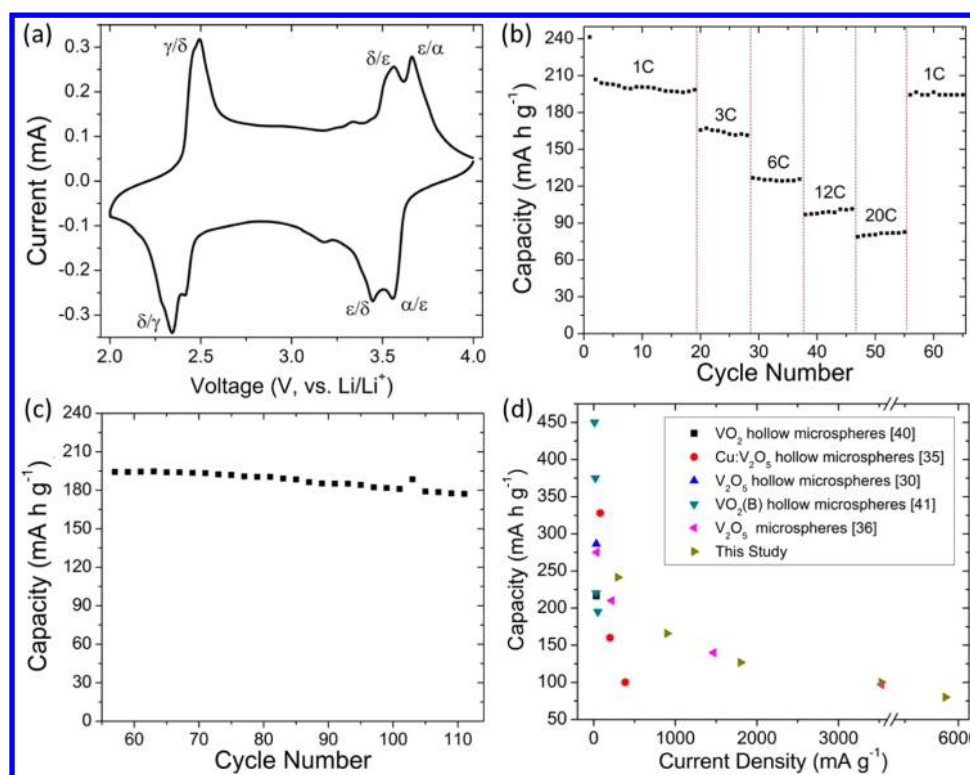
Figure 5. (a) Cyclic voltammogram obtained at a scan rate of 0.2 mV s^{-1}; (b) rate performance of the V$_2$O$_5$ microsphere electrode at 1, 3, 6, 12, and 20C; (c) cycle stability of the V$_2$O$_5$ microsphere electrode when tested at 1C after rate performance testing; (d) rate performance comparison with other VO$_x$ microspheres as gathered from the literature.

enced during the Li$^+$ intercalation/deintercalation process, thereby improving the cyclic stability by alleviating any strain the electrode incurs; second, the large surface area and decreased Li$^+$ diffusion distance in hollow nanostructured electrodes greatly enhance the specific capacity while decreasing the packing density.[27,35,36] To date, there have only been a few reports of hollow V$_2$O$_5$ microspheres, but the precursor materials or experimental conditions used in these studies are either expensive or time-consuming. Additionally, the 1C current density in these studies is often defined as the insertion of one Li ion per V$_2$O$_5$ formula over the course of one hour, or 150 mA g^{-1}.[30,35,36] Therefore, a study concerning inexpensive, easy processable hollow V$_2$O$_5$ microspheres that demonstrate excellent electrochemical performance has yet to be reported.

The cycling performance of the prepared electrodes was tested within the voltage range of 2.0−3.8 V. The selected voltage window was chosen to avoid the formation of the irreversible ω-phase of Li$_x$V$_2$O$_5$ (2 < x < 3) that occurs at lower depth of discharge, thereby improving the cycle stability.[37] It should be noted that only the V$_2$O$_5$ mass was included in the calculation of the specific capacity of the electrode. As shown in Figure 5a, several well-defined redox peaks are observed between 3.4 and 2.3 V (vs Li/Li$^+$) in the initial cyclic voltammogram collected at a rate of 0.2 mV s^{-1}. These peaks were attributed to the insertion/extraction of lithium ions into the host structure, and the corresponding phase transitions have been labeled. Figure 5b shows the discharge capacities of the V$_2$O$_5$ microspheres at current densities of 300 (1C), 900 (3C), 1800 (6C), 3600 (12C), and 6000 (20C) mA g^{-1}, which were 241, 165, 127, 96, and 78 mA h g^{-1}, respectively. As previously mentioned, these values are considerably higher than others reported in the literature.

There was a small degree of irreversible capacity loss from 241 to 206 mA h g^{-1} occurring between the first and second discharge at 1C (Figure S4, Supporting Information), which can be attributed to remnant localized strain effects from solid-state amorphization or pulverization experienced during cycling.[38,39] The cycle stability of the cell was then analyzed following rate performance cycling, the results of which are shown in Figure 5c. The V$_2$O$_5$ microspheres were reasonably stable at a discharge rate of 1C with capacity values of approximately 190 mA h g^{-1}, even after being cycled at a high discharge rate of 20C. The Li-ion capacity values of the V$_2$O$_5$ microspheres synthesized in this study were compared to similar structures listed in the literature. Figure 5d shows the findings of this comparison; it is evident that the V$_2$O$_5$ microspheres reported here are far superior to any other microspherical VO$_x$ materials to date, especially at higher current densities.[40,41] It should be noted that the conductive additive loadings in these studies were all equal to or greater than the amount of conductive additive used in this study (12%).

The enhanced electrochemical high-rate and cycling performance of the hollow microspheres can be attributed to the improved kinetic properties as a result of their morphology. The hollow microsphere morphology composed of nanoparticles eases the transportation of lithium ions by increasing the ratio of active material surface area to electrolyte and ensures rapid ionic and electronic conduction throughout the electrode. Also, the void within hollow nanostructured materials can alleviate any localized volume change experienced during the Li$^+$ intercalation/deintercalation process, thereby decreasing the degree of pulverization the active material experiences upon cycling, further improving the cycle stability.

CONCLUSIONS

In conclusion, a highly scalable and reproducible template-free process was developed for the synthesis of hollow V_2O_5 microspheres composed of aggregated nanoparticles. It was proposed that N_2 microbubbles formed during the reaction acted as aggregation centers for the synthesized vanadyl glycolate nanoparticles, resulting in the observed hollow microsphere morphology. The synthesized material showed excellent cycle stability and high discharge rate performance, which can be ascribed to the thin shell that ensures fast phase penetration between the electrolyte and active material and a short lithium ion migration distance during intercalation/deintercalation, and the morphological void which accommodates cycling induced localized strain. The current results clearly demonstrate that hollow V_2O_5 microspheres are well suited for application as cathode materials for Li-ion batteries.

ASSOCIATED CONTENT

Ⓢ Supporting Information

Additional electron micrographs, electrochemical data, and N_2 sorption analyses. This material is available free of charge via the Internet at http://pubs.acs.org.

AUTHOR INFORMATION

Corresponding Author
*E-mail: gzcao@u.washington.edu.

Notes
The authors declare no competing financial interest.

ACKNOWLEDGMENTS

REFERENCES

(1) Antonietti, M.; Ozin, G. A. Chem.—Eur. J. 2004, 10, 28.
(2) Colfen, H.; Antonietti, M. Angew. Chem., Int. Ed. 2005, 44, 5576.
(3) Liu, J.; Cao, G.; Yang, Z.; Wang, D.; Dubois, D.; Zhou, X.; Graff, G. L.; Pederson, L. R.; Zhang, J.-G. ChemSusChem 2008, 1, 676.
(4) Kim, F.; Connor, S.; Song, H.; Kuykendall, T.; Yang, P. D. Angew. Chem., Int. Ed. 2004, 43, 3673.
(5) Shen, L.; Uchaker, E.; Yuan, C.; Nie, P.; Zhang, M.; Zhang, X.; Cao, G. ACS Appl. Mater. Interfaces 2012, 4, 2985.
(6) Shen, L.; Zhang, X.; Uchaker, E.; Yuan, C.; Cao, G. Adv. Energy Mater. 2012, 2, 691.
(7) Feldmann, C.; Jungk, H. O. Angew. Chem., Int. Ed. 2001, 40, 359.
(8) Ragupathy, P.; Shivakumara, S.; Vasan, H. N.; Munichandraiah, N. J. Phys. Chem. C 2008, 112, 16700.
(9) Jiang, X. C.; Herricks, T.; Xia, Y. N. Adv. Mater. 2003, 15, 1205.
(10) Jiang, X. C.; Wang, Y. L.; Herricks, T.; Xia, Y. N. J. Mater. Chem. 2004, 14, 695.
(11) Wiley, B.; Herricks, T.; Sun, Y. G.; Xia, Y. N. Nano Lett. 2004, 4, 1733.
(12) Liu, C.; Wu, X. W.; Klemmer, T.; Shukla, N.; Yang, X. M.; Weller, D.; Roy, A. G.; Tanase, M.; Laughlin, D. J. Phys. Chem. B 2004, 108, 6121.
(13) Chen, J. Y.; Herricks, T.; Geissler, M.; Xia, Y. N. J. Am. Chem. Soc. 2004, 126, 10854.
(14) Pileni, M. P. Nat. Mater. 2003, 2, 145.
(15) Caswell, K. K.; Bender, C. M.; Murphy, C. J. Nano Lett. 2003, 3, 667.
(16) Herricks, T.; Chen, J. Y.; Xia, Y. N. Nano Lett. 2004, 4, 2367.
(17) Ho, C. M.; Yu, J. C.; Kwong, T.; Mak, A. C.; Lai, S. Y. Chem. Mater. 2005, 17, 4514.
(18) Zhou, N.; Liu, Y.; Li, J.; Uchaker, E.; Liu, S.; Huang, K.; Cao, G. J. Power Sources 2012, 213, 100.
(19) Sun, Y. G.; Yin, Y. D.; Mayers, B. T.; Herricks, T.; Xia, Y. N. Chem. Mater. 2002, 14, 4736.
(20) Caruso, F.; Caruso, R. A.; Mohwald, H. Science 1998, 282, 1111.
(21) Liu, J.; Xue, D. Nanoscale Res. Lett. 2010, 5, 1525.
(22) Shen, L. F.; Li, H. S.; Uchaker, E.; Zhang, X. G.; Cao, G. Z. Nano Lett. 2012, 5673−5678.
(23) Fu, H.; Jiang, X.; Yang, X.; Yu, A.; Su, D.; Wang, G. J. Nanopart. Res. 2012, 14, 871.
(24) Liu, Y.; Uchaker, E.; Zhou, N.; Li, J.; Zhang, Q.; Cao, G. J. Mater. Chem. 2012, 24439.
(25) Weeks, C.; Song, Y. N.; Suzuki, M.; Chernova, N. A.; Zavalij, P. Y.; Whittingham, M. S. J. Mater. Chem. 2003, 13, 1420.
(26) Sun, Y. G.; Xia, Y. N. Adv. Mater. 2002, 14, 833.
(27) Luo, J.; Cheng, L.; Xia, Y. Electrochem. Commun. 2007, 9, 1404.
(28) Lamer, V. K.; Dinegar, R. H. J. Am. Chem. Soc. 1950, 72, 4847.
(29) Peng, Q.; Dong, Y. J.; Li, Y. D. Angew. Chem., Int. Ed. 2003, 42, 3027.
(30) Cao, A. M.; Hu, J. S.; Liang, H. P.; Wan, L. J. Angew. Chem., Int. Ed. 2005, 44, 4391.
(31) Ocana, M.; Rodriguezclemente, R.; Serna, C. J. Adv. Mater. 1995, 7, 212.
(32) Talledo, A.; Granqvist, C. G. J. Appl. Phys. 1995, 77, 4655.
(33) Whittingham, M. S. Science 1976, 192, 1126.
(34) Wang, Y.; Cao, G. Z. Chem. Mater. 2006, 18, 2787.
(35) Zhu, D.; Liu, H.; Lv, L.; Yao, Y. D.; Yang, W. Z. Scr. Mater. 2008, 59, 642.
(36) Wang, S.; Lu, Z.; Wang, D.; Li, C.; Chen, C.; Yin, Y. J. Mater. Chem. 2011, 21, 6365.
(37) Liu, Y. Y.; Li, J. G.; Zhang, Q. F.; Zhou, N.; Uchaker, E.; Cao, G. Z. Electrochem. Commun. 2011, 13, 1276.
(38) Limthongkul, P.; Jang, Y. I.; Dudney, N. J.; Chiang, Y. M. Acta Mater. 2003, 51, 1103.
(39) Liu, Y.; Hudak, N. S.; Huber, D. L.; Limmer, S. J.; Sullivan, J. P.; Huang, J. Y. Nano Lett. 2011, 11, 4188.
(40) Kong, F. Y.; Li, M.; Yao, X. Y.; Xu, J. M.; Wang, A. D.; Liu, Z. P.; Li, G. H. CrystEngComm 2012, 14, 3858.
(41) Liu, H.; Wang, Y.; Wang, K.; Hosono, E.; Zhou, H. J. Mater. Chem. 2009, 19, 2835.